

1 **New Phenomenological Quality Criteria for Continuous Casting of Steel Based on** 2 **Solidification and Microstructure Tool IDS**

3 Seppo Louhenkilpi^{1,2)}, Jyrki Miettinen¹⁾, Ville-Valtteri Visuri^{1*)}, Mahesh C. Somani³⁾,
4 Sami Koskenniska³⁾, and Timo Fabritius¹⁾

5

6 1) Process Metallurgy Research Unit, University of Oulu, PO Box 4300, 90014 University of
7 Oulu, Finland

8 2) Department of Chemical and Metallurgical Engineering, Aalto University, PO Box 16200,
9 00076 Aalto, Finland

10 3) Materials and Mechanical Engineering Research Unit, University of Oulu, PO Box 4200, 90014
11 University of Oulu, Finland

12 * Corresponding author. E-mail: ville-valtteri.visuri@oulu.fi

13

14 **ABSTRACT**

15

16 Although the formation of defects in continuous casting has been studied for several decades, a deeper
17 understanding and improved quality prediction concepts are needed to correlate the defects with the
18 actual steel compositions, machine data and casting parameters. The aim of this work was to derive
19 new quality criteria based on steel composition and cooling pattern for continuous casting and for the
20 subsequent cooling and reheating processes. The criteria were devised based on the outputs of
21 multiphysics simulation tools for online casting applications. The developed criteria were found to
22 be good predictors of whether a steel grade combined with a given cooling pattern is prone to a
23 specific defect. The criteria useful in providing a theoretical justification as to why certain defects
24 form or would form, and can be used for devising practical solutions to avoid them. In practice, the
25 final determination of whether a defect will form depends on the cumulative impact of various single
26 quality criteria combined with the models/data describing the mechanical and thermal stresses
27 forming. The criteria proposed are applicable as part of online quality prediction systems in casting
28 machines. In this paper, new quality criteria were proposed for different kind of cracking-related and
29 gas defects along with case examples. In further work, the criteria will be used to develop rule-based
30 online control systems, in which cumulative effects of individual quality criteria are combined with
31 data from mechanical and thermal stress calculations.

32

33 **Keywords:** continuous casting, simulation, quality criteria

34 I INTRODUCTION

35

36 Research and development efforts in the field of continuous casting of steel are being continued
37 intensively to achieve better quality of the cast product, higher productivity and strict control on
38 chemistry and cleanliness, besides the need for smooth operation of the casting process that is linked
39 to the ladle operations and hot rolling. To this end, computational simulation and modelling of
40 physico-chemical phenomena taking place during the casting process has greatly helped in solving
41 the practical problems encountered in industrial casters and facilitated the improvement of process
42 practices and control accuracy [1,2,3].

43

44 Many defects introduced during the casting process are influenced by the steel grade, machine design
45 and condition as well as the casting operation. Although the formation of defects has been studied for
46 several decades, a deeper understanding of their nature of formation and improved quality prediction
47 concepts are inevitably needed to correlate the evolution of defects with the actual steel compositions,
48 machine data and casting parameters. Understanding the mechanisms of defect formation is important
49 for minimizing their number and size, particularly in the light of new innovative compositions in use
50 in recent years.

51

52 Today many sensors have been installed to the casting machines. Nevertheless, the quality of the
53 castings cannot be measured directly using these installed sensors and hence higher-level
54 computerized quality control systems, which predict and assess the quality of the cast product, are
55 needed. The traditional rating is typically based upon the comparison of actual measurements from
56 the process (e.g. mold level, casting speed) against the existing standards in predefined disposition
57 data tables, which are configured through statistical analyses or through plant experience. This
58 approach often works adequately, but has several drawbacks. The main problem is that it is difficult
59 to relate the defects only with the signals of the sensors and it is, therefore, tedious, time-consuming
60 and costly to define the disposition tables accurately. This is especially the case for new quality
61 specifications or while making changes to the casting conditions / parameters. Extensive work has
62 carried out to develop more advanced quality prediction systems and criteria for defects based on
63 advanced tools [4–17]. Many of the previously-published criteria presented in the literature are based
64 on thermo-mechanical calculations, especially for cracking type of defects [7, 8, 10, 11, 15]. The
65 typical approach is that if the total mechanical strain exceeds a critical value, a crack will form. These
66 models do not proceed from the mechanism of defects although such a method could be used to
67 describe various factors that may cause defects. It is also difficult to obtain high temperature

68 mechanical data, especially creep data, and to know the critical strain/stress values as a function of
69 steel composition. In addition, no real-time dynamic method for calculating stress and strain state in
70 continuous casting is available. Especially for hot cracking, some solidification modelling based
71 criteria have been also developed as an example the CSC criterion [18]. The simplest solidification
72 based hot cracking criteria are based on the solidification interval and they take into account only the
73 alloy composition. Some models calculate the whole solidification interval ($\Delta T_{LS} = T_L - T_S$) for
74 evaluating the crack sensitivities, but some only a smaller part of it and typically they consider the
75 smaller range just above the solidus (brittle temperature range, BTR). BTR is typically defined as
76 $BTR = T_{ZST} - T_{ZDT}$, where T_{ZST} is the zero-strength temperature and T_{ZDT} is the zero-ductility
77 temperature. The index increases with the solidification interval or the brittle temperature range,
78 respectively. Nevertheless, there are no generally valid criteria published that link defects in
79 continuous casting to steel grade, machine design and condition. Quality prediction systems based on
80 artificial intelligence systems are also presented [4, 9, 16]. But, the model presented does not proceed
81 from the mechanisms of defect formation either. In conclusion, still higher level science-based
82 fundamental models are lacking, which could simulate online the most important phenomena
83 occurring in continuous casting and relate them to defect formations. Such computational modeling
84 plays an important role in generating deeper understanding of defects and their formation. Once
85 developed, these kinds of models can be used as an integral part of the on-line quality prediction
86 systems in casting machines. They could also provide an insight into the type and nature of defect
87 formations and even lead to practical solutions to alleviate them.

88
89 The aim of this work was to derive new quality criteria for computerized quality control systems
90 based on the in-house computational tools developed for continuous casting. To this end, a
91 solidification and cooling related, multiphysics microstructure simulations package IDS was
92 employed for calculating the properties required by various indices as illustrated later. The IDS
93 simulates the microstructural phenomena occurring during solidification, cooling and also reheating,
94 thus covering a range of processes from continuous casting to hot rolling based on the steel
95 composition and cooling/heating rates. To account for the effects of different cooling patterns on
96 quality criteria, the IDS is usually coupled with CastManager, a transient three-dimensional on-line
97 heat transfer model, and its offline version Tempsimu. These models are based on the fundamental
98 phenomena, but are designed to be sufficiently fast for online use, making the approach realizable at
99 steelmaking plants. The final determination if a defect is forming in practice depends on the
100 cumulative impact of various single quality criteria combined with the models/data describing the
101 mechanical and thermal stresses forming. The tools developed, the new single quality criteria and

102 case examples are presented. So far, the quality criteria have mainly been developed for different
103 kinds of cracks.
104

105 **II IDS AND CASTMANAGER/TEMPSIMU TOOLS**

106

107 IDS is a thermodynamic-kinetic-empirical software package, which has been developed since 1984
108 to simulate solidification and cooling/heating related microstructural phenomena, such as phase
109 transformations, solute microsegregation, inclusion and precipitate formation, precipitate dissolution,
110 grain growth and austenite decomposition [19-23]. The package has since been validated with
111 extensive data of solidification experiments [19, 21, 24]. Recently, the IDS database has been
112 extended to enable improved simulations new steel grades [25, 26].

113

114 IDS can be applied to different physical states right from the liquid state to the solidified, as-cast state
115 cooled down to room temperature and also during the reheating/homogenization treatments in a
116 reheating furnace. The rate of cooling or reheating, of course, can vary. Due to the very short
117 calculation times, the tool is fairly suitable for online applications. The solute elements covered by
118 IDS calculations are C, Si, Mn, P, S, Cr, Mo, Ni, Al, Cu, Nb, Ti, V, Ca, Ce, Mg, B, O, N and H [22].
119 The IDS tool consists of several modules and not all the elements are included in every module.

120

121 The phases simulated by IDS are: δ -ferrite, α -ferrite, eutectic ferrite, austenite, cementite, pearlite,
122 bainite, α -martensite (bcc structure) and ϵ -martensite (hcp structure). The inputs of the simulation are
123 the nominal composition of the steel and cooling and heating rates. The present IDS software package
124 includes several calculation modules [19] for simulating the solidification and the austenite
125 decomposition process, including the formation of inclusions and precipitates, and for calculating
126 temperature functions for material properties. The most recent of these modules is the QIN module,
127 which calculates steel quality indices providing information about the sensitivity to various casting
128 problems, such as cracking.

129

130 CastManager and Tempsimu are heat transfer modelling software packages for the continuous casting
131 of steel [22, 23]. CastManager is for online applications, while Tempsimu is a steady state model.
132 The material data required for the calculations is provided by the IDS tool. The computing times of
133 the IDS and CastManager are short, and the programs have now been integrated together in one online
134 concept, which has recently been installed in the automation systems of four slab casters in Finland.

135

136

137 **III NEW QUALITY CRITERIA FOR CONTINUOUS CASTING AND SUBSEQUENT**
138 **COOLING AND REHEATING PROCESSES**

139

140 In this chapter, new quality criteria for solidification during continuous casting and subsequent
141 reheating process are introduced. They are based mainly on the calculated results of the IDS tool.
142 Several IDS results or phenomena can be related to the occurrence of casting defects and accordingly,
143 many single quality criteria have now been developed. The cooling rates or cooling patterns for the
144 IDS are calculated using the heat transfer models, Tempsimu or CastManager. Whether a steel grade
145 is prone to a specific defect will typically depend on the cumulative impact of various single quality
146 criteria. **Table 1** shows some of the main defects as well as the quality criteria associated with them.

147 **Table 1.** Proposed main criterion indices for different types of **cracking** defects.

Defect	Criterion										
	Q _I SHE	Q _I STR	Q _I SOL	Q _I DUC	Q _I GRA	Q _I BUB	Q _I POR	Q _I COOL	Q _I COLD	Q _I HEAT	Tramp elements
Longitudinal surface cracking, facial and corner	X	X	X								
Transverse corner cracking	X	X		X	X						X
Bleeding	X	X									
Hot spots, depressions	X										
Near-surface pinholes						X					
Internal gas porosity, blowholes							X				
Star cracks	X			X							X
Cracking during cooling after continuous casting								X			
Cold cracking									X		
Cracking during reheating in the reheating furnace										X	

148

149 A. Q_{ISTR} and Q_{SHE} indices

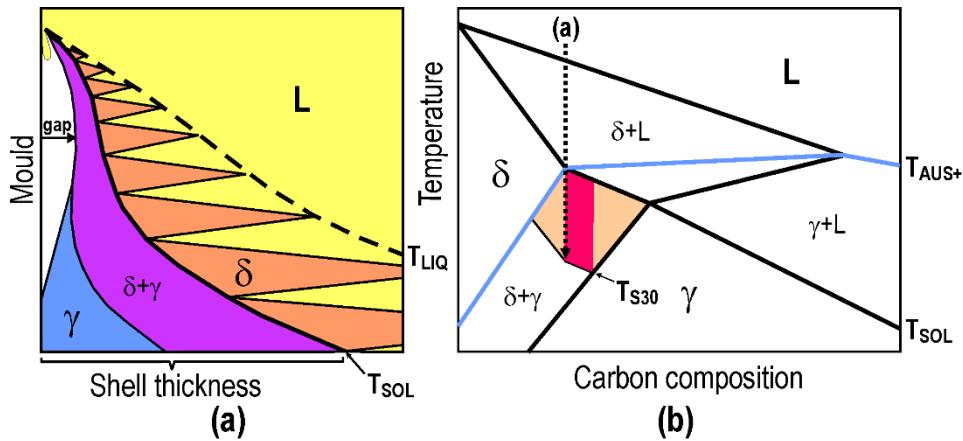
150

151 The Q_{ISTR} and Q_{SHE} indices defined and developed in this work are associated with the phase
 152 transformation from delta ferrite to austenite during the last stage of solidification (Q_{ISTR}) and
 153 just after the solidification (Q_{SHE}). As delta ferrite has a lower density than austenite, the
 154 volume change taking place during phase transformation causes contraction in the solidifying
 155 shell resulting in corresponding transformation stresses and strains in the structure. If the
 156 amount of ferrite transforming to austenite is high, thus resulting in large volume contraction,
 157 then the steel becomes very sensitive to various types of quality problems.

158

159 **Figure 1** shows schematically the phenomenon in context with the index Q_{SHE} . It is well
 160 known that the phase transformation from delta ferrite to austenite just below the solidus may
 161 cause severe quality problems, especially in the mold area [3, 27]. The reaction of delta ferrite
 162 takes place in the red zone of **Figure 1b**, which provides a schematic presentation of a kinetic
 163 pseudo-binary phase diagram calculated with IDS for a multicomponent carbon steel.

164



165

166 **Figure 1.** Detachment of the shell due to the delta ferrite/austenite transformation (a) and the
 167 red temperature zone, where shell growth is disturbed (b). The worst cases are in the deep red
 168 zone. Temperature T_{s30} denotes $T_{SOL} - 30$ °C.

169

170 To provide a numerical value for this phenomenon, the following index was devised:

171

$$Q_{SHE} = f_{SOL}^{\sigma} - f_{MAX}^{\sigma}, \quad (1)$$

172

173 where f_{SOL}^{σ} is the delta ferrite fraction at the solidus temperature and f_{MAX}^{σ} is the maximal delta
 174 ferrite fraction between T_{SOL} and $T_{SOL} - 30$ °C. Both the ferrite fractions are calculated with the

175 IDS tool, based on the steel composition and the cooling rate. Index QI_{SHE} is typically between
176 0 and 1 and increasing the value indicates a higher risk of problems. Typically, the QI_{SHE} index
177 is high for carbon contents between about 0.08 and 0.15 wt-% in carbon steels, but alloying and
178 tramp elements tend to change that carbon range. For stainless steels, the highest risk is at the
179 Cr/Ni equivalent ratio of about 1.8. In these steels, the index values are lower than in carbon
180 steels, because the ferrite/austenite transformation is much slower. Irrespective of the steel type,
181 the risk of problems can be reduced by using a correct casting powder and mold taper and also
182 by avoiding those steel compositions (within specified composition tolerance ranges), which
183 give the highest values for this index.

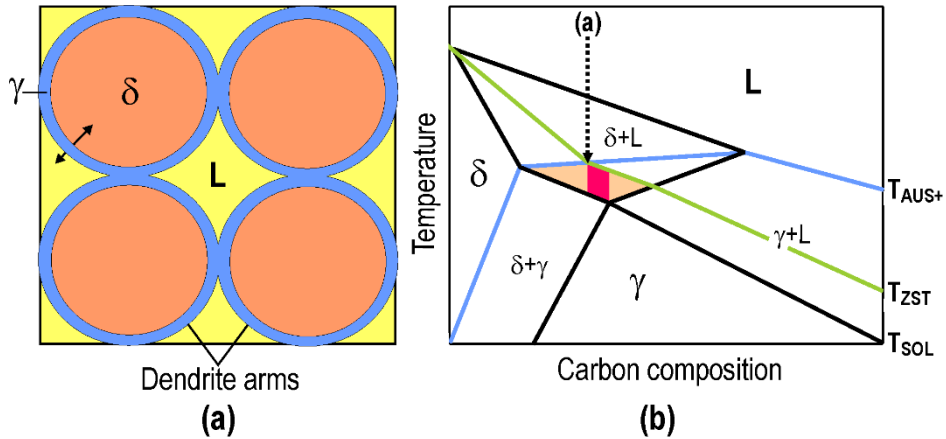
184

185 The effect of a high QI_{SHE} value can also be seen during the mold heat transfer. Typically, the
186 mold heat transfer is quite uniform if solidification is either purely ferritic or austenitic. The
187 shell formed in this way, when still thin, places itself tightly against the mold wall, which enables
188 increased heat transfer from the strand to the mold. However, if austenite starts to form in the
189 thin ferritic shell just formed (at or slightly below the solidus temperature), i.e., when QI_{SHE} has
190 a high value, the shell can detach itself locally from the mold [3]. Consequently, heat transfer is
191 weakened and becomes uneven. This can lead to different kinds of surface, subsurface and
192 internal defects and in the worst case, even to breakouts. Hot cracking may be forming, when
193 the surface of the detached shell is rapidly heated, leading to high tensile stresses at the
194 solidification front. Because the longitudinal surface cracks are also initiated as hot cracking, a
195 high QI_{SHE} value also means a higher risk of longitudinal surface cracking. The shell heating
196 due to its detachment leads to a coarser shell structure at the surface, which increases the risk of
197 defects, too.

198

199 During the peritectic transformation above the solidus, the austenite is forming from ferrite and
200 liquid. A volume change does take place in that reaction when the austenite layer forms between
201 the liquid and ferrite (see **Figure 2a**). During solidification of a steel, its local strengthening
202 can be assumed to start at a zero-strength temperature (T_{ZST}), as the solid fraction reaches a
203 value of about $f_s = 0.75$. At this moment, the dendrite arms will be in contact with the
204 neighboring dendrite arms and the solidification structure starts to get strength. If austenite
205 starts to form (from the liquid phase and ferrite) between solid fractions of about 0.75 and 1
206 (1=solidus), the corresponding volume change due to phase transformation causes stresses and
207 strains in the dendritic structure, i.e. the strengthening will be disturbed. This increases the risk
208 of surface and internal cracks. Typical defects forming, among others, include transverse corner

209 cracking, longitudinal surface cracking, hot cracking, bleeding, etc. The disturbing effect on
 210 strengthening suggests that the stronger it becomes, the more vigorous is the disappearance of
 211 delta ferrite between T_{ZST} and T_{SOL} . Typically, the worst problems occur around the peritectic
 212 point, which is approximately 0.18 wt-% carbon [3, 28, 29, 30]. However, the alloying and
 213 tramp elements tend to change the carbon range. For stainless steels, the greatest risk is when
 214 the Cr/Ni equivalent ratio is about 1.8 [31]
 215



216
 217 **Figure 2.** Background of quality index QI_{STR} . Formation of austenite layer between the liquid
 218 phase and ferrite just after strengthening (a) and the red temperature zone, where strengthening
 219 is disturbed (b). **The worst cases are in the deep red zone.**

220
 221 QI_{STR} index is defined as
 222

$$QI_{STR} = f_{MAX}^{\sigma} - f_{SOL}^{\sigma}, \quad (2)$$

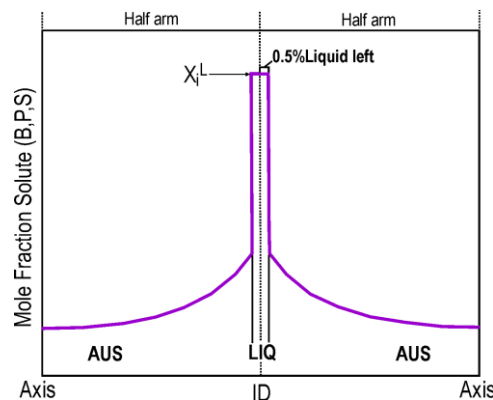
223
 224 where f_{MAX}^{σ} is the maximal delta ferrite fraction between T_{ZST} and T_{SOL} and f_{SOL}^{σ} is the delta
 225 ferrite fraction at the solidus. Again, both the ferrite fractions are calculated with the IDS tool,
 226 depending on the steel composition and the cooling rate. **Figure 2a** shows schematically the
 227 phenomenon behind this index. The worst cases are in the deep red zone shown in **Figure 2b**.
 228

229 B. Index QI_{SOL}

230

231 The QI_{SOL} criterion describes the reduced hot ductility around the solidus because of the strong
232 enrichment of some specific elements, such as S, P and B [3, 29, 30], in the interdendritic liquid
233 (**Figure 3**). The higher the austenite fraction that forms during solidification, the stronger the
234 solute enrichment that takes place in the liquid phase. For this reason, the problem is most
235 relevant in high carbon and austenitic stainless steels, particularly those containing little or no
236 ferrite during solidification. In addition, enrichment of sulfur and oxygen in liquid may lead to
237 the formation of a sulfur and oxygen rich liquid phase. This can strongly reduce the ductility.
238 So far, IDS simulates the formation of liquid-state compounds of (Fe,Mn)S and B_2O_3 . For
239 specific steel compositions, some elements, such as Nb, Si and Ti, may also increase the
240 sensitivity to hot cracking. Normal calculations carried out using the IDS routinely consider
241 how these elements affect the solidification phenomena as phase transformations, segregations,
242 compound formations (with C, N, S and others) and the effects on hot cracking is taken in this
243 way.

244



245

246 **Figure 3.** Background of quality index QI_{SOL} . Solute enrichments (e.g. S, P and B) and the
247 fraction of the liquid-state (Fe,Mn)S in the last liquid drop at the solidus (0.5% liquid left) for
248 the derivation of QI_{SOL} index.

249

250 Sulfur enrichment in the liquid can be reduced with manganese, but the Mn/S ratio in that case
251 needs to be adequately high, and should be even higher, when the steel is strongly austenitic
252 [32]. If the ratio is not sufficiently high, it may lead to the formation of sulfide (Fe,Mn)S, which
253 may contain too much iron. This can lower the solidus of the sulfide, thus leading to the
254 formation of liquid sulfide films at the grain boundaries, which strongly reduces the ductility.
255 MnS alone has a higher melting point and is not very harmful in the absence of Fe. Some rare-

256 earth elements have also been found to be highly effective in binding the excess sulfur, and also
257 phosphorus, to stable compounds [33]. In addition, there are also solute elements, like copper
258 and tin, which tend to form a solute-rich liquid phase, thus reducing the ductility.

259

260 IDS calculates the dissolved compositions (mole fractions, x_i^L) of all solutes (such as S, P, B,
261 Nb, Ti) in the residual liquid and the fraction of the liquid state sulfide, (Fe,Mn)S, marked as
262 $f^{(Fe,Mn)SL}$. All these terms are calculated, when 0.5% liquid is left in the interdendritic region
263 (**Figure 3**). The present QI_{SOL} index is expressed as

264

$$QI_{SOL} = f(x_i^L, f^{(Fe,Mn)SL}) \quad (3)$$

265

266 It is to be noted that the function type itself is still open, which will be fixed in due time, by
267 correlating the hot cracking indices with the experimental data and/or empirical knowledge.
268 The effect of the liquid state B_2O_3 is also under study.

269

270 C. Index QI_{GRA}

271

272 A coarse grain structure is known to increase the risk of crack formation. In general, the stresses
273 in the solid structure will concentrate at the softer phase. Typically, the grain boundary is softer
274 than the grain itself, especially if soft ferrite bands or chain-like precipitates are present at the
275 boundary. In large grains, the external stresses concentrating at the softer and weaker grain
276 boundaries are higher than those in fine grains. Reducing grain size has a strong effect on
277 improving the ductility in both ferrite and austenite. It increases the number of triple points
278 making the structure more ductile and also increases the grain boundary area so that the
279 precipitation density at the grain boundary area is reduced [34].

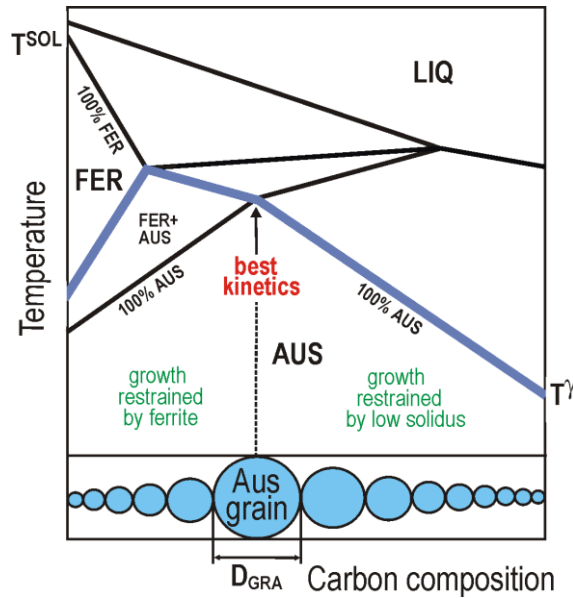
280

281 There are many reasons for the occurrence of grain growth during the casting process. If the
282 earlier mentioned QI_{SHE} index is high, there is a big risk of uneven heat transfer in the mold as
283 well as the formation of hot spots, which lead to shell reheating and formation of large grains
284 in these hot spot locations. At high temperatures, the grains may grow quite fast in fully
285 austenitic steels also, due to the kinetic conditions favorable for their growth.

286

287 **Figure 4** schematically presents the austenite grain size as a function of carbon content. The
288 coarsest grains are obtained with 100% austenite structure at the highest possible solidus

289 temperature. In carbon steels, this corresponds to the peritectic point of about 0.18 wt-% C. At
 290 lower carbon compositions, the grains remain finer due to the pass through the FER+AUS zone,
 291 as ferrite restrains the austenite grain growth. Besides, grain growth is also restrained by
 292 precipitate formation at the boundaries.
 293



294
 295 **Figure 4.** Background of quality index QI_{GRA} . Fastest austenite grain growth occurs in the
 296 composition region corresponding to 0.18 wt-% carbon with best possible kinetics (diffusion).
 297

298 The lowering of ductility due to the formation of large austenite grain size (thus leading to poor
 299 quality) is described with the index QI_{GRA} as given below:
 300

$$QI_{GRA} = D_{GRA} \quad (4)$$

301
 302 where D_{GRA} is the austenite grain size (μm) at temperature $T_{SOL} - 200$ °C, calculated by IDS.
 303 The IDS tool enables the calculation of grain size from the solidus temperature to room
 304 temperature taking into account the effect of ferrite as well as precipitate formation during the
 305 cooling/heating process involved. Because of other reasons, the grain size can also be high for
 306 carbon steels with approximately 0.1 wt-% carbon or for equivalent stainless steels. In that case,
 307 the criterion QI_{SHE} describes the phenomenon.
 308
 309

310 D. Indices QI_{BUB} and QI_{POR}

311

312 During the solidification of steels, gas bubbles (H_2 , N_2 and CO), may form from the liquid
313 phase. If a gas bubble forms above the zero-strength temperature, where interdendritic liquid
314 films are still connected to the main liquid, the bubble will assumedly flow up to the meniscus.
315 These kinds of bubbles may be very harmful. The bubbles may form pinholes near the strand
316 surface or go alongside with the casting powder into the mold and the steel shell and interfere
317 with the lubrication. This may even cause breakouts because the bubbles in the casting powder
318 locally reduce the heat transfer drastically. If the bubbles form below the zero-strength
319 temperature, they presumably stay in the solid shell and cause gas porosity. The reduced strand
320 quality caused by the gas bubbles flowing up to the meniscus area (QI_{BUB}) or by the gas porosity
321 formation (QI_{POR}) is described by the following formula:

322

$$QI_{POR} = 1 - \exp[-10000 \cdot (f^{H_2(g)} + f^{N_2(g)} + f^{CO(g)})] \quad (4)$$

323

324 where $f^{H_2(g)}$, $f^{N_2(g)}$ and $f^{CO(g)}$ are either the mole fractions of the corresponding gases at the
325 zero-strength temperature leading to $QI_{BUB} = QI_{XXX}$, or the gas fractions formed below the zero-
326 strength and the solidus temperature leading to $QI_{POR} = QI_{XXX}$. In both cases, the gas fractions
327 are calculated with IDS. Note that the results depend on the pressure defined as $P = P_{ex} -$
328 $f_S(P_{ex} - P_{mus})$, where P_{ex} is the ferrostatic pressure at the liquidus temperature, f_S is the solid
329 fraction in the mushy zone (IDS output) and P_{mus} is the effective pressure at the solidus
330 temperature (i.e., with $f_S = 1$). The ferrostatic pressure is calculated as $P_{ex} = 1 + \rho gh/10^5$
331 (bar), where ρ is the liquid density, g is the gravity constant and h is the liquid height. The
332 liquid height is obtained from the heat transfer calculations. Hence, the main idea is that the
333 ferrostatic pressure increases in the first place, which resists gas formation down to the liquidus
334 temperature. Consequently, the shrinking mushy zone (solidification shrinkage) decreases the
335 ferrostatic pressure to the P_{mus} level at the solidus temperature, which promotes gas formation.
336 In the same way, it is also possible to model gas formation in the shrinkage pores (voids), which
337 typically form in the center of the strand. In that case, the pressure P should be close to zero.
338 The quality index can also be calculated separately for different gas bubble types, i.e., H_2 , N_2
339 and CO .

340

341 E. Index Q_{IDUC}

342

343 In microalloyed steel, transverse corner cracking is a common defect type, especially in vertical
344 bending casting machines. This defect is strongly influenced by the presence of microalloying
345 elements that form precipitates with C, N and S [3, 31, 34]. When the strand is bent or
346 straightened, transverse corner cracks occur, as the strand corners approach the vicinity of the
347 low-ductility temperature regime of the steel. The causes of crack formation are attributed to
348 the chain-like precipitations and the film-like proeutectoid ferrite along the austenite grain
349 boundaries. The cracks are normally located in (deep) oscillation marks. At the bottom of the
350 deep oscillation marks, the grains are found to be quite coarse and it is obvious that large grain
351 size increases sensitivity to all kinds of cracking.

352

353 The main reason for the increased sensitivity of steel towards transverse corner cracking is the
354 occurrence of precipitations, but typically this is not the only reason. Formation of relatively
355 coarse grains (described by $Q_{I_{GRA}}$, $Q_{I_{SHE}}$) as well as generation of internal phase transformation
356 stresses during delta ferrite to austenite phase transformation (described by $Q_{I_{STR}}$ or $Q_{I_{SHE}}$)
357 also contribute to transverse corner cracking. If the indices $Q_{I_{STR}}$ and $Q_{I_{SHE}}$ are small, then the
358 chances of transverse corner cracking are greatly reduced.

359

360 Chain-like precipitations and film-like proeutectoid ferrite reduce the steel ductility at lower
361 temperatures. The most detrimental precipitate responsible for transverse corner cracking is
362 known to be Nb(C,N). As small particles along the austenite grain boundaries, these precipitates
363 weaken the bond between the austenite grains, particularly in the presence of film-like
364 proeutectoid ferrite. Other precipitates, such as V(C,N), Ti(C,N), AlN_7 and (Mn,Fe)S, can also
365 effectively reduce the ductility. However, a clear understanding of the combined effects of Nb,
366 V, Ti, Al and Mn-on the occurrence of precipitations and corresponding loss of ductility is not
367 so straightforward and is very complicated. For instance, vanadium and titanium may have both
368 positive and negative effects.

369

370 Nitrogen content and the particle size too play a significant role. A low nitrogen level tends to
371 reduce the amount of nitrides and in general, the cracking sensitivity too. In addition, large
372 precipitate particles are not so harmful, when compared to chain-like particles. Typically, if a
373 precipitate forms at a high temperature and the subsequent cooling rate is slow (hence, more
374 time for the precipitates to grow), the particles will be coarser and less harmful. On the other

375 hand, V(C,N) and Ti(C,N) precipitates may also serve as nucleation points for Nb(C,N), thus
376 leading to the formation of coarse, complex precipitates. On the other hand, some steel grades
377 without Nb microalloying may still be very sensitive to corner cracking. For instance, vanadium
378 and aluminum bearing steels with high N content may be very sensitive to corner cracking. To
379 comprehensively study the nature of the problem and to understand the effects of microalloying
380 elements, a thermodynamic-kinetic model, such as IDS, is mandatory, as well as also
381 knowledge of the 2nd ductility trough and its strength.

382
383 The IDS tool facilitates calculation of the mole fractions of single precipitates (e.g. Nb (C,N),
384 V(C,N), Ti(C,N), AlN, BN, (Mn,Fe)S, and CaS) as a function of steel composition and cooling
385 rate. The precipitates formed in the temperature range from 1200 °C to the temperature $T_{Ar3} -$
386 30 °C (T_{Ar3} is the start temperature for austenite decomposition) are the most harmful for this
387 defect type. Below $T_{Ar3} - 30$ °C, the ferrite band between the austenite grains becomes so thick
388 that it can withstand bending or straightening stresses. IDS calculates also the T_{Ae3} and T_{Ar3}
389 temperatures (T_{Ae3} is the *equilibrium* start temperature for austenite decomposition). We
390 assume that during bending or straightening, proeutectoid ferrite starts to form at T_{Ae3} as a
391 strain-induced ferrite. Moreover, we assume that the ductility is recovered at about $T_{Ar3} - 30$
392 °C, as mentioned before. Some elements, such as P or B, increase the cohesion of the austenite
393 grain boundary, which is known to have positive effects on ductility.

394
395 These type of effects can be considered in the quality prediction models using empirical
396 relationships. It is also known that only the film-like proeutectoid ferrite at the austenite grain
397 boundary is harmful. If the ferrite forms in other ways, for instance, in the form of acicular or
398 Widmanstätten ferrite, the problem can be reduced. IDS assumes that the ferrite forms typically
399 as proeutectoid ferrite at the austenite grain boundaries. It is noteworthy that the precipitates
400 causing transverse corner cracking may also cause mid-face transverse cracking [30].

401
402 It is very difficult to make only one simple mathematical formula to predict the sensitivity of a
403 steel grade to transverse corner cracking, as the phenomena behind the cracking are quite
404 complicated. To predict the sensitivity, cumulative effects of the single indexes (such as QI_{SHE} ,
405 QI_{STR} , QI_{GRA} , QI_{DUC}) and other relevant information should be considered. This is the next
406 future step in our research. Rule based algorithms or artificial intelligence system will be used.

409 F. *Indices for phenomena after continuous casting: for cooling, hydrogen induced cracking,*
410 *reheating (QI_{COOL} , QI_{COLD} and QI_{HEAT})*

411

412 The cracking tendency during cooling after continuous casting is typically associated with
413 martensite formation, which is an athermal transformation process. Martensite is a hard but
414 brittle phase and its hardness increases with increasing carbon content. Martensite containing
415 steels, whose carbon content is lower than about 0.10 wt-% are softer and less susceptible to
416 cracks. Martensite has a density lower than austenite and is accompanied by an increase in
417 volume, combined with the shear strains following phase transformation, causing large stresses
418 and strains in the structure. Besides, during cooling, thermal stresses are also generated in the
419 structure. Accordingly, the steel surface and corners cool faster than the inner core, which
420 causes large tensile stresses on the surface.

421

422 Cracking can occur especially if there are softer phases (ferrite) along the prior austenite grain
423 boundaries and the rest of the structure is hard martensite and/or bainite. Thermal stresses
424 combined with the internal stresses from martensite transformation are concentrated in the
425 softer ferrite band. Cracking may take place, especially in the surface where the thermal stresses
426 lead to tensile strains. The risk is still higher if there is chain-like precipitation in the softer
427 ferrite band, which hinders the grain boundary sliding. Consequently, the susceptibility to
428 cracking increases. A low cooling rate is beneficial, because the thermal stresses will be smaller
429 and the amount of martensite or bainite formation is reduced or completely eliminated.

430

431 Prior austenite grain size and carbon content have noticeable effect on cracking. The strains
432 generated on the boundaries of coarser grains will be higher than in finer grains, and with higher
433 carbon content in the steel, the martensite is not only harder, but very brittle, too. So far as
434 bainite is concerned, the transformation temperature is relatively higher, and hence the shape
435 deformation due to bainite formation is relaxed by the plastic deformation of the adjacent
436 austenite. So, bainite is considered less harmful than martensite, but it is also harder than ferrite.
437 It must also be noted that the presence of retained austenite between the martensite laths can
438 effectively block crack propagation. The QI_{COOL} index, therefore, predicts the sensitivity of a
439 steel grade to surface cracking during cooling after continuous casting. If it is high, slow cooling
440 is needed. So far, we do not have a single formula for the QI_{COOL} index, but the following data
441 is calculated for it:

442

- 443 • Amount of ferrite, martensite, bainite, retained austenite at 25 °C
- 444 • The temperature of the disappearance of delta or proeutectoid ferrite from the structure
- 445 (if zero at room temperature).
- 446 • Amount of precipitates in the prior austenite grain boundary
- 447 • Prior austenite grain size
- 448 • Carbon content

449

450 Another type of cracking occurring during cooling, particularly in the steels of the storing hall,
451 is cold cracking (or hydrogen induced cracking). The solubility of H in ferrite is considerably
452 lower than that in austenite and therefore, cold cracking is typically related to the ferrite phases,
453 especially with the hard and brittle martensite, and of course the original amount of hydrogen
454 in the melt. Especially in martensite, the dislocation density is high and these dislocations act
455 as nucleation sites for the hydrogen gas, forming as $2[\text{H}]^{\text{Fe}} \rightarrow \text{H}_2 (\text{g})$. With lower carbon content
456 (<0.1 wt-% C), the martensite is not so hard and brittle, and in most cases, not so sensitive to
457 cracking.

458

459 H_2 pressure together with cooling induced transformation stresses and the residual stresses due
460 to storing may cause severe cracking. Even very low hydrogen content (1–2 ppm) may cause
461 problems and in the strands cooled in the storing hall, new cracks can form over several days
462 (delayed cracking). Typically, cold cracking takes place at temperatures below 200 °C and to
463 calculate this index, IDS uses the following output data:

464

- 465 • Excess H level in the structure at 25 °C
- 466 • Amount of martensite, bainite, ferrite, retained austenite at 25 °C
- 467 • Carbon content of the steel

468

469 Cracking may also take place also during reheating. This is strongly associated with the low
470 ductility phases, such as hard and brittle martensite, and/or grain boundary ferrite bands with
471 chain-like precipitates. The thermal expansion is so high that the low ductility phases cannot
472 withstand the resulting stresses during reheating. The volume change from martensite to
473 austenite becomes negative, i.e., there is shrinkage in this reaction, which also increases the
474 tension stresses in the structure. Lower heating rates are needed for these kinds of steels. Similar
475 data as required during cooling (QI_{COOL}) is calculated for the index QI_{HEAT} , too.

476

477 **IV RESULTS AND DISCUSSION**

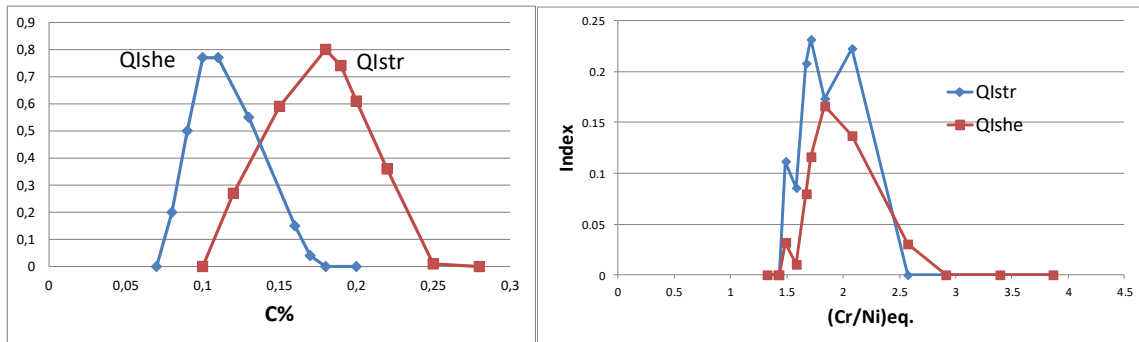
478

479 A. QI_{SHE} and QI_{STR}

480

481 **Figure 5a** shows the calculated values of the QI_{SHE} and QI_{STR} indices for a fixed low alloyed
482 steel composition with varying carbon content, whereas **Figure 5b** presents the corresponding
483 values for different stainless steel grades as a function of $(Cr/Ni)_{eq}$. For the carbon steel, the
484 highest values of the QI_{SHE} and QI_{STR} indices are attained at carbon contents of about 0.1 wt-
485 % and 0.18 wt-%, respectively. However, as mentioned earlier, alloying influences the peak
486 value locations very strongly. The QI_{STR} values in **Figure 5a** fit well, among other things, with
487 the practical observation that steels containing 0.17 to 0.24% carbon are particularly crack
488 sensitive [29,30]

489



490

491 **Figure 5.** a) Indices QI_{STR} and QI_{SHE} for a fixed low alloyed steel composition with varying
492 carbon content. The indices are partly overlapping, b) corresponding QI_{STR} and QI_{SHE} indices
493 for stainless steels showing nearly complete overlapping.

494

495 For stainless steels, the highest values are at about $(Cr/Ni)_{eq}$ of 1.80 and the corresponding
496 compositions are significantly prone to surface defects. It can also be seen that unlike in the
497 case of carbon steels, the indices QI_{STR} and QI_{SHE} are fully overlapping and the values are lower
498 than those of carbon steels.

499

500 For further testing the QI_{STR} index, we calculated its value for two industrial steel compositions
501 (steel A and B), which are very sensitive to transverse corner cracking. For steel A the QI_{STR}
502 value was 0.99 and for steel B 1.00, which are practically the highest possible values the index
503 can have. If the QI_{STR} value is high and has certain precipitates (such as AlN , $V(C,N)$,
504 $Nb(C,N)$), these may adversely affect the steel ductility at lower temperatures, when the strand
505 is bent or unbent and the steels, therefore, become very sensitive to transverse corner cracking.

506 It is believed that a similar situation prevails with the QI_{SHE} and practically with the whole
507 overlapping area of QI_{SHE} and QI_{STR} . However, if the QI_{STR} and/or QI_{SHE} indices are low, then
508 seemingly the precipitates alone do not make the steel sensitive to cracking.

509

510 There are other parameters too affecting the occurrence of transverse corner cracking, such as
511 deep oscillation marks, grain size, etc. and these should also be taken into account when making
512 a rule-based quality prediction model for transverse corner cracking. At the bottom of the deep
513 oscillation marks grains are typically higher than at the low oscillation marks. As mentioned
514 before, in large grains, the external stresses concentrating at the softer and weaker grain
515 boundaries are higher than those in fine grains.

516

517 *B. Bleeding*

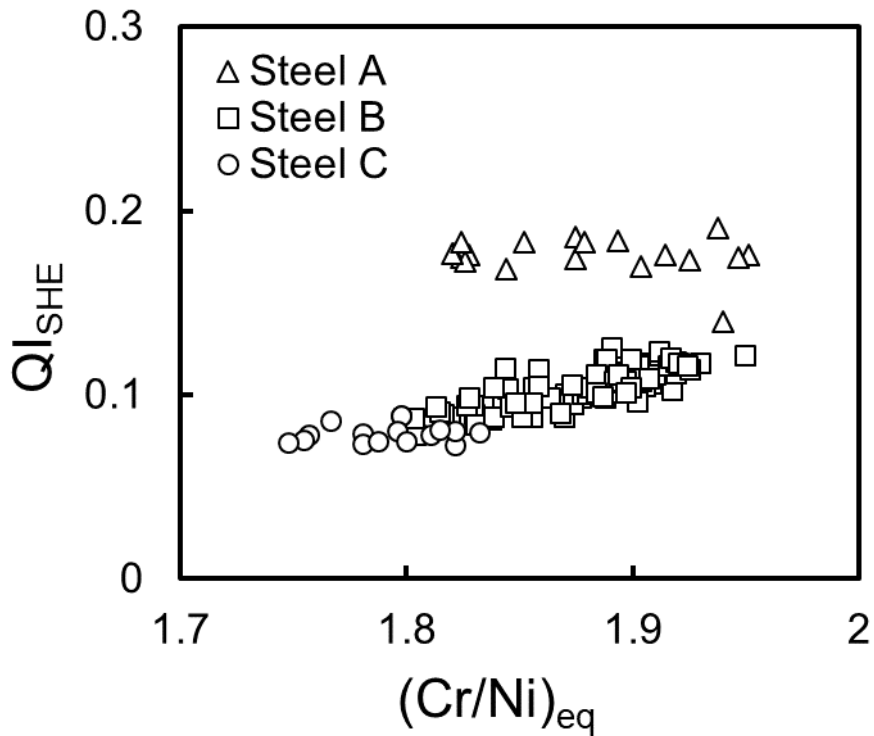
518

519 Another industrial case study was carried out with stainless steels. Bleeding is a serious surface
520 defect that occurs in the mold. The molten steel breaks through the shell inside the mold and
521 unlike in the case of a breakout, this liquid quickly spreads in the gap and freezes. Although
522 this heals the shell, it leaves a distinct patch or scab on the steel surface that can delaminate
523 during rolling. Also, liquid overflow over the solidifying shell may cause a similar defect.

524

525 Three stainless steel grades, viz., A, B and C, prone to bleeding effect, were studied to provide
526 an insight into the phenomenon. These steels are normal austenitic stainless steel grades with
527 $(Cr/Ni)_{eq}$ from about 1.75 to 1.95 with typically approximately 17.5 wt-% Cr and 6.5–8 wt-%
528 Ni. Steel A, which is the most sensitive for bleeding, has 17.5 wt-% Cr, 6.5 wt-% Ni and high
529 N content. Figure 6 shows the calculation results. Based on statistical defect analysis one of
530 them (steel A) is clearly the most sensitive to bleeding and steel C is a bit less sensitive than B.
531 All the compositions, in general, are in the high-risk domain close to $(Cr/Ni)_{eq} \approx 1.80$ and hence,
532 are sensitive to various kinds of defects, as mentioned before. But for the steel grade most
533 sensitive to bleeding (A), the QI_{SHE} values (blue points) are clearly higher than those for grades
534 B and C. Hence it is quite evident that QI_{SHE} is evidently correlated to bleeding defect, too. To
535 avoid the occurrence of such defects, it is prudent to avoid the highest QI_{SHE} values, if possible.
536 In addition, deep oscillation marks have also been found to have a direct correlation with the
537 occurrence of bleeding and should be avoided.

538



539

540 **Figure 6.** QI_{SHE} values for three stainless steel grades (A, B, C), which all are sensitive to
 541 bleeding, based on the statistical defect analysis made in the industry. Steel grade A is distinctly
 542 the most sensitive for bleeding and steel grade C is a bit less sensitive than grade B. QI_{STR} index
 543 gives very similar results.

544

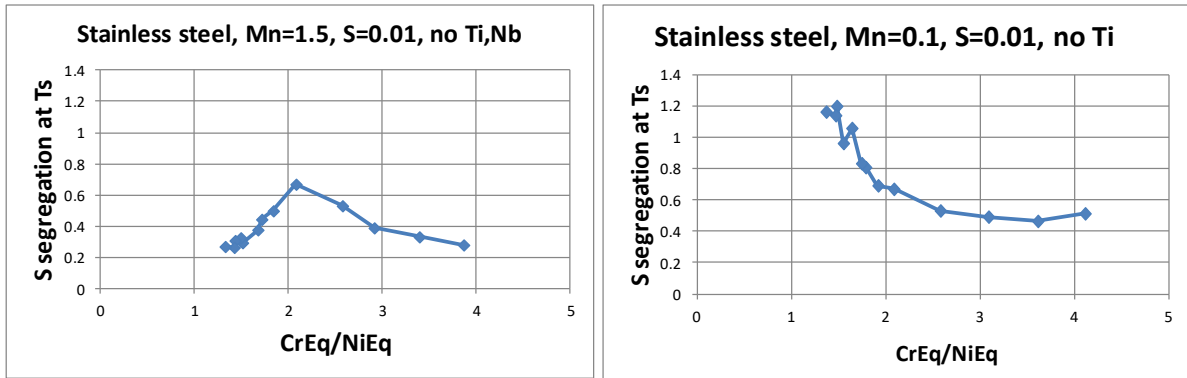
545 *C. Hot cracking*

546

547 Hot cracking in ferritic stainless steels is not as common as in austenitic stainless steels, because
 548 of the comparatively lesser extent of microsegregation in ferritic steels. An example of sulfur
 549 microsegregation can be seen in **Figure 7**. Calculations were made for different stainless steel
 550 grades using the IDS tool. While the sulfur content was maintained at the same level, i.e., $S =$
 551 0.01 wt%, the manganese content was either 0.1 wt-% or 1.5 wt-%. Referring to the right-hand-
 552 side of **Figure 7**, this stainless steel contains very low manganese (i.e. $Mn = 0.1$ wt-%) and
 553 hence, the Mn/S ratio is only 10. It can be seen that the sulfur enrichment at solidus increases
 554 exponentially as $(Cr/Ni)_{eq}$ decreases. This is because the amount of austenite formation during
 555 solidification increases with the lowering of $(Cr/Ni)_{eq}$.

556

557



558

559 **Figure 7.** Calculated segregation of sulfur in two different stainless steel grades. Left: not prone
560 to hot cracking; right: very prone to hot cracking.

561

562 It is well known that when the $(Cr/Ni)_{eq}$ in stainless steels is lower than about 1.5-1.7 [35], the
563 risk of hot cracking increases strongly, as can be discerned from the right-hand side of **Figure**
564 **7.** Therefore, the presence of sulfur in the steel reduces the ductility. This can be prevented if
565 the nominal S and P contents in the steel are low ($S+P < \text{about } 0.01-0.02\%$) and also, the Mn
566 content is raised to a higher level that binds S to form MnS, as depicted in the left-hand of
567 **Figure 7** (Mn = 1.5%). It can be seen that with higher Mn, the microsegregation of S is reduced
568 effectively, when $(Cr/Ni)_{eq}$ is lower than about 2, and also, the tendency to hot cracking
569 decreases drastically. It must, however, be noted that ferritic stainless steels may also become
570 susceptible to hot cracking if the S and P contents are high. In addition, the ferritic grades
571 stabilized with Nb and Ti, might also be very susceptible to hot cracking, because Nb and Ti
572 have a strong tendency to form compounds with C and N and hence, reduce the hot ductility.
573 These phenomena can also be predicted with IDS-aided calculations.

574

575 The low ductility around the solidus temperature is not the only reason for the occurrence of
576 hot cracking. Stresses are also needed. Various types of stresses also promote hot cracking, such
577 as those resulting from phase transformations, mechanical stresses from the casting process
578 manifesting as bending and unbending stresses, and thermal stresses. The phase transformation
579 stresses related to the solidification process can be described with the quality indices, QI_{STR} and
580 QI_{SHE} as described earlier. Hence, the hot cracking phenomena can be predicted using the
581 QI_{STR} , QI_{SHE} and QI_{SOL} indices coupled with the formulas describing the thermal and
582 mechanical stresses from the casting process. The grain size also has some effects, because
583 coarse grain structure reduces the ductility as mentioned earlier.

584

585 One industrial carbon steel grade, which was very prone to hot cracking, was further studied.
586 For that steel, the QI_{STR} index was found to be very high, 0.98 and the grain size was very
587 coarse, too (QI_{GRA} index). The microsegregation of sulfur and phosphorus was also very high
588 in this steel grade: the final enrichment was 60 and 10 times the nominal content for sulfur and
589 phosphorus, respectively. Though the Mn/S ratio was high, the formation of (Mn,Fe)S was
590 delayed until very close to the solidus temperature, thus it was unable to prevent the loss of hot
591 ductility. The IDS tool and the developed criteria could, therefore, predict the occurrence of hot
592 cracking sensitivity in this steel composition very well.

593

594 *D. Cooling after continuous casting*

595

596 Two steel grades, steel A (0.19 wt-% C, 1 wt-% Cr steel) and B (0.21 wt-% C, 0.85 wt-% Cr
597 steel), which happened to be very crack sensitive during cooling following continuous casting,
598 were modeled using the IDS tool. Steel A is The steels can be produced at extremely low
599 cooling rates, but cracking does take place at higher cooling rates. Two cooling rates were
600 considered for modelling the solidification process following continuous casting: 0.02 °C/s
601 (slow) and 1 °C/s (high). With the slow cooling rate (0.02 °C/s), the following phase fractions
602 were obtained for the two steels at 25 °C:

603

- 604 • Steel A: Proeutectoid ferrite 8.3%, pearlite 77.7%, bainite 12.2%, and martensite 1.6%,
605 and
- 606 • Steel B: Proeutectoid ferrite 10.9%, pearlite 89%. Therefore, at a slow cooling rate, the
607 structure of the two steels is mainly ferritic-pearlitic and hence, is free from crack
608 sensitivity.

609

610 In contrast, at the high cooling rate, the phase fractions were: Steel A: Proeutectoid ferrite 1.4%,
611 bainite 67.2%, and martensite 30.3%, and steel B: Proeutectoid ferrite 2.1%, bainite 79.8 %,
612 and martensite 17.5%, This suggests that at a high cooling rate, the structure is essentially
613 pearlite-free with a narrow ferritic band and mainly consists of harder phases, bainite and
614 martensite.

615

616 With a further increase in the cooling rate, a greater fraction of martensite is formed, too. Hence,
617 it can be easily construed that the structures can become crack-sensitive with faster cooling
618 rates. Seemingly, the narrow ferrite band with chain-like precipitates and hard internal grain

619 structure adversely affects steels with a greater propensity to cracking at higher cooling rates.
620 In general, a fully martensitic (+bainitic) structure may become quite sensitive to cracking and
621 should be cooled very slowly.

622

623 *E. Cold cracking*

624

625 As a corollary to crack-sensitivity of steels at high cooling rates following continuous casting
626 (QI_{COOL} index), it has been observed that they become sensitive to cold cracking (i.e., hydrogen
627 cracking), too. According to a common welding formula, the above-mentioned steel grades, A
628 and B, which are sensitive to cracking at faster cooling rates, have also been considered very
629 sensitive to hydrogen induced cracking. Anyhow, according to the IDS calculation results, at
630 slow cooling rates, these steels are neither crack-sensitive during solidification following
631 continuous casting, nor are prone to cold cracking.

632

633 *F. Cracking during reheating*

634

635 Five continuously cast steel grades (steel A, B, C, D and E), which were considered very crack
636 sensitive during fast heating in a reheating furnace, were modeled using the IDS tool. The tool
637 was used to simulate continuous casting and subsequent cooling to room temperature.

638

639 Following cooling at $0.02\text{ }^{\circ}\text{C/s}$ after continuous casting, the microstructure of three castings A,
640 B and E revealed essentially a mixture of proeutectoid ferrite and pearlite with proeutectoid
641 ferrite contents varying in a narrow range of 4.8%, 6.3% and 4.6%, respectively. At a still higher
642 cooling rate ($1\text{ }^{\circ}\text{C/s}$), the structures were similarly free of any bainite or martensite, but the
643 proeutectoid ferrite bands were narrower.

644

645 Under similar cooling conditions, steels C and D showed essentially a bainitic-martensitic
646 microstructure with narrow bands of proeutectoid ferrite and/or cementite. All these five steel
647 grades were very close to the eutectoid point in respect of carbon content. It means that narrow
648 bands of the proeutectoid ferrite /cementite in the structures render them crack-sensitive and
649 during fast reheating cracks may easily form. This is the case with a high cooling rate too after
650 continuous casting. These steels should be cooled down, and then reheated in the reheating
651 furnace slowly. Chain-like precipitates in the narrow bands combined with the hard grain
652 interior make these structures even more sensitive to cracking. Hence, adequate care must be

653 taken in reheating the structures of steels with compositions close to the eutectoid point. For
654 comparison of these results, a cold cracking formula for welding was also used. According to
655 the cold cracking formula for welding, steels B, C, and D are very prone to cold cracking,
656 whereas steels A and D are in the boundary area between low and high sensitivity to cracking.

657

658 **V CONCLUSIONS**

659

660 The formation of defects in continuous casting is largely influenced by the steel grade, machine
661 design, and casting operation. Even though the formation mechanisms may be well known, the
662 prediction of defects is still quite difficult and requires high-level computational tools, which
663 are able to account for and calculate the most important phenomena in continuous casting and
664 link them to the occurrence of defects. Another typical problem is that a single phenomenon or
665 criterion cannot alone predict the sensitivity or formation of a defect, because the cumulative
666 effects of the phenomena is unknown.

667

668 In this work, the new quality criteria were derived from the calculated results of the IDS tool
669 based on the steel composition and cooling rates. Several quality indices have already been
670 developed and tested successfully, so far in off-line mode, as presented in this paper. Some
671 criteria have also been developed for cooling and reheating processes taking place following
672 the continuous casting process. The developed criteria can be used as important segments in the
673 online quality prediction systems in casting machines. An additional benefit is that they are able
674 to provide fairly accurate reasons why the defects forms or would form, and practical proposals
675 in order to avoid them. The work will be continued with rule based control systems to take into
676 account more accurately the cumulative effects of the important phenomena. Using this
677 approach, it would be possible to calculate in advance the optimal target compositions for
678 certain defect-sensitive steel grades in order to avoid high index values.

679

680 **ACKNOWLEDGEMENTS**

681

682 The funding of this research activity within the framework of Genome of Steel (Profi3) by the
683 Academy of Finland through project #311934 is gratefully acknowledged. V.-V. Visuri thanks
684 the Walter Ahlström foundation for financial support.

685

686

687 **REFERENCES**

688

- 689 1. B. G. Thomas, *Steel Res. Int.*, 2018, vol. 89, 1700312.
- 690 2. K. C. Mills, P. Ramirez-Lopez, P. D. Lee, B. Santillana, B. G. Thomas, R. Morales,
691 *Ironmaking Steelmaking*, 41, 242 (2014).
- 692 3. S. Louhenkilpi: *Continuous Casting of Steel*, in: *Treatise on Process Metallurgy Volume*
693 *3: Industrial Processes* (Elsevier, Oxford, United Kingdom, 2014) pp. 373–434.
- 694 4. Y. Kong, D. Chen, Q. Liu, and M. Long, *Metals*, 9, 587 (2019).
- 695 5. C. M. Chimani, H. Resch, K. Mörwald, and O. Kolednik, *Ironmaking Steelmaking*, 32,
696 75 (2005)
- 697 6. P. Ershun, Y. Liang, J. J. Shi, and T. Chang, *J. Manuf. Sci. Eng.*, 131, 1 (2009)
- 698 7. F. M. Du, X. D. Wang, Y. Liu, J. J. Wei, and M. Yao, *Steel Res. Int.*, 88, 1 (2017)
- 699 8. J. E. Lee, T. J. Yeo, K. H. Oh, J. K. Yoon, and U. Yoon, *Metall. Mater. Trans. A*, 31, 225
700 (2000).
- 701 9. C. A. Santos, J. A. Spim, and A. Garcia, *Eng. Appl. Artif. Intell.*, 16, 511 (2003).
- 702 10. Y. M. Won, T. Yeo, D. J. Seol, and K. H. Oh, *Metall. Mater. Trans. B*, 31, 779 (2000)
- 703 11. M. O. El-Bealy, *Metall. Mater. Trans. B*, 43, 1488 (2002).
- 704 12. K. Dou, J. S. Qing, L. Wang, X. F. Zhang, B. Wang, Q. Liu, and H. B. Dong, *Acta Metall.*
705 *Sin.*, 50, 1505 (2014).
- 706 13. M. S. Kulkarni and A. S. Babu, *J. Mater. Process. Technol.*, 166, 294 (2005).
- 707 14. J. H. Kim, T. J. Yeo, K. H. Oh, and D. N. Lee, *ISIJ Int.*, 36, 284 (1996).
- 708 15. Z. Q. Han, K. K. Cai, and B. C. Liu, *ISIJ Int.*, 41, 1473 (2001).
- 709 16. X. D. Wang, M. Yao, and X. F. Chen, *ISIJ Int.*, 46, 1047 (2006).
- 710 17. R. Pierer, S. Michelic, C. Bernhard, and C. Chimani: *A hot tearing criterion for the*
711 *continuous casting process*, Proceedings of the 3rd International Steel Conference on
712 *New Developments in Metallurgical Process Technologies* (Steel Institute VDEh,
713 Düsseldorf, Germany, 2007) pp. 893–900.
- 714 18. T. W. Clyne, M. Wolf, W. Kurz, *Metall. Trans B*, 13,259 (1982).
- 715 19. J. Miettinen, S. Louhenkilpi, V.-V. Visuri, and T. Fabritius, *IOP Conf. Ser.: Mater. Sci.*
716 *Eng*, 529, 012063 (2019).
- 717 20. J. Miettinen, S. Louhenkilpi, H. Kytönen, and J. Laine, *Math. Comput. Simulat.*, 80, 1536
718 (2010)
- 719 21. P. Presoly, C. Bernhard, N. Fuchs, J. Miettinen, S. Louhenkilpi, and J. Laine: *Further*
720 *development and validation of IDS by means of selected experiments*, Proceedings of the

- 721 9th Continuous Casting Conference (The Austrian Society for Metallurgy and Materials,
722 Vienna, Austria, 2017).
- 723 22. S. Louhenkilpi, J. Miettinen, J. Laine, R. Vesanen, I. Rentola, J. Moilanen, V.-V. Visuri,
724 E.-P. Heikkinen, and A. Jokilaakso, *IOP Conf. Ser.: Mater. Sci. Eng.*, 529, 012051 (2019).
- 725 23. S. Louhenkilpi, J. Laine, J. Miettinen, and R. Vesanen, *Mater. Sci. Forum*, 762, 691
726 (2013).
- 727 24. J. Miettinen: *Validation of IDS calculations with experimental data*, internal report,
728 (Casim Consulting Oy, Espoo, Finland, 2017).
- 729 25. J. Miettinen, V.-V. Visuri, and T. Fabritius, *Acta Univ. Oul. C Technica*, 704, 2019.
- 730 26. J. Miettinen, V.-V. Visuri, T. Fabritius, N. Milcheva, and G. Vassilev, *Arch. Metall.*
731 *Mater.*, 64, 451 (2019).
- 732 27. A. Grill and J. K. Brimacombe, *Ironmaking and Steelmaking*, 3, 76 (1976).
- 733 28. P. K. Agarwal, R. W. Pugh, and J. K. Brimacombe: *Case study of Spray Design for a*
734 *Continuous Billet Caster*, Continuous Casting, Volume 2: Heat Flow, Solidification and
735 Crack Formation (Iron & Steel Society of AIME, Warrendale, PA, USA, 1984) pp. 153–
736 167.
- 737 29. J. K. Brimacombe, E. B. Hawbolt, and F. Weinberg: *Formation of off-corner internal*
738 *cracks in the continuously-cast billets*, Continuous Casting, Volume 2: Heat Flow,
739 Solidification and Crack Formation (Iron & Steel Society of AIME, Warrendale, PA,
740 USA, 1984) pp. 229–238.
- 741 30. J. K. Brimacombe, K. Sorimachi, *Metall Trans. B*, 8, 489 (1997).
- 742 31. M. Wolf: *Continuous Casting, Volume 9: Initial Solidification and Strand Surface*
743 *Quality of Peritectic Steels* (Iron & Steel Society of AIME, Warrendale, PA, USA, 1997)
744 pp. 1–57.
- 745 32. H. F. Schrewe: *Continuous Casting of Steel* (Verlag Stahleisen mbH, Dusseldorf,
746 Germany, 1987), pp. 139-140.
- 747 33. M. Opiela, A. Grajcar: *Modification of Non-Metallic Inclusions by Rare-Earth Elements*
748 *in Microalloyed Steels*, Archives of Foundry Engineering, vol 12 issue 2/2012, pp. 125-
749 134
- 750 34. B. Mintz and S. Yue: *The hot ductility test for assessing the likelihood of transverse*
751 *cracking during continuous casting of steel*, Continuous Casting, Volume 8: Transverse
752 *cracking in continuously cast products* (Iron & Steel Society of AIME, Warrendale, PA,
753 USA, 1997) pp. 233–240.

754 35. V. P. Kujanpää, N. J. Suutala, T. K. Takalo, and T. J. I. Moisio, *Metall. Constr.*, 12, 282
755 (1980)

756 **LIST OF FIGURES**

757

758 **Figure 8.** Detachment of the shell due to the delta ferrite/austenite transformation (a) and the
759 red temperature zone, where shell growth is disturbed (b). **The worst cases are in the red zone.**
760 Temperature T_{s30} denotes $T_{SOL} - 30$ °C.

761

762 **Figure 9.** Background of quality index QI_{STR} . Formation of austenite layer between the liquid
763 phase and ferrite just after strengthening (a) and the red temperature zone, where strengthening
764 is disturbed (b). **The worst cases are in the red zone.**

765

766 **Figure 3.** Background of quality index QI_{SOL} . Solute enrichments (e.g. S, P and B) and the
767 fraction of the liquid-state (Fe,Mn)S in the last liquid drop at the solidus (0.5% liquid left) for
768 the derivation of QI_{SOL} index.

769

770 **Figure 4.** Background of quality index QI_{GRA} . Fastest austenite grain growth occurs in the
771 composition region corresponding to 0.18 wt-% carbon with best possible kinetics (diffusion).

772

773 **Figure 5.** a) Indices QI_{STR} and QI_{SHE} for a fixed low alloyed steel composition with varying
774 carbon content. The indices are partly overlapping, b) Corresponding QI_{STR} and QI_{SHE} indices
775 for stainless steels showing nearly complete overlapping.

776

777 **Figure 10.** QI_{SHE} values for three stainless steel grades (A, B, C), which all are sensitive to
778 bleeding, based on the statistical defect analysis made in the industry. Steel grade A is distinctly
779 the most sensitive for bleeding and steel grade C is a bit less sensitive than grade B. QI_{STR} index
780 gives very similar results.

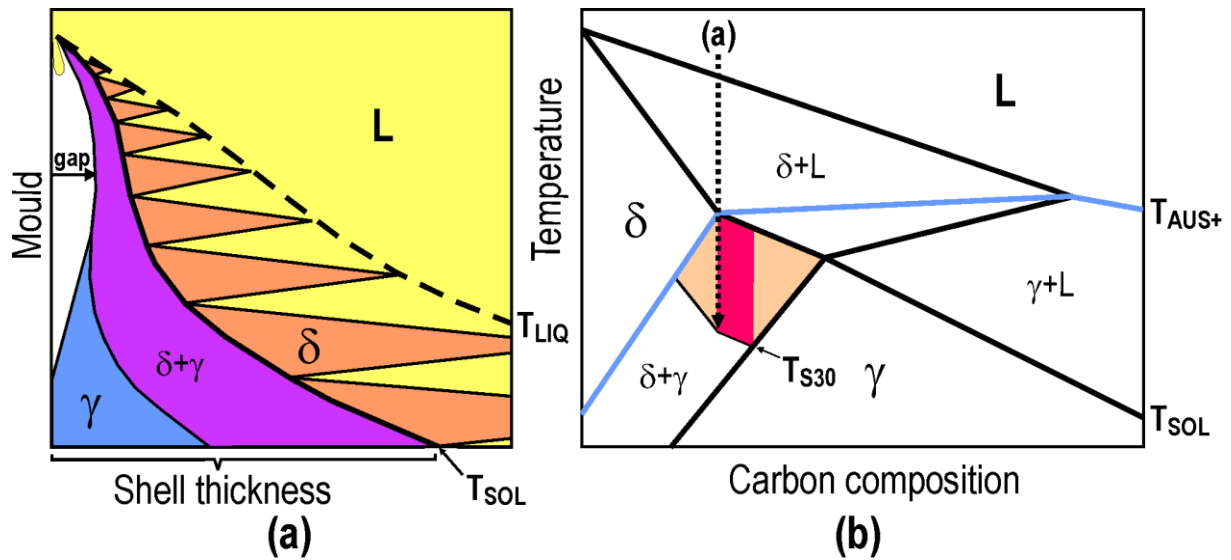
781

782 **Figure 11.** Calculated segregation of sulfur in two different stainless steel grades. Left: not
783 prone to hot cracking; right: very prone to hot cracking.

784

785

786

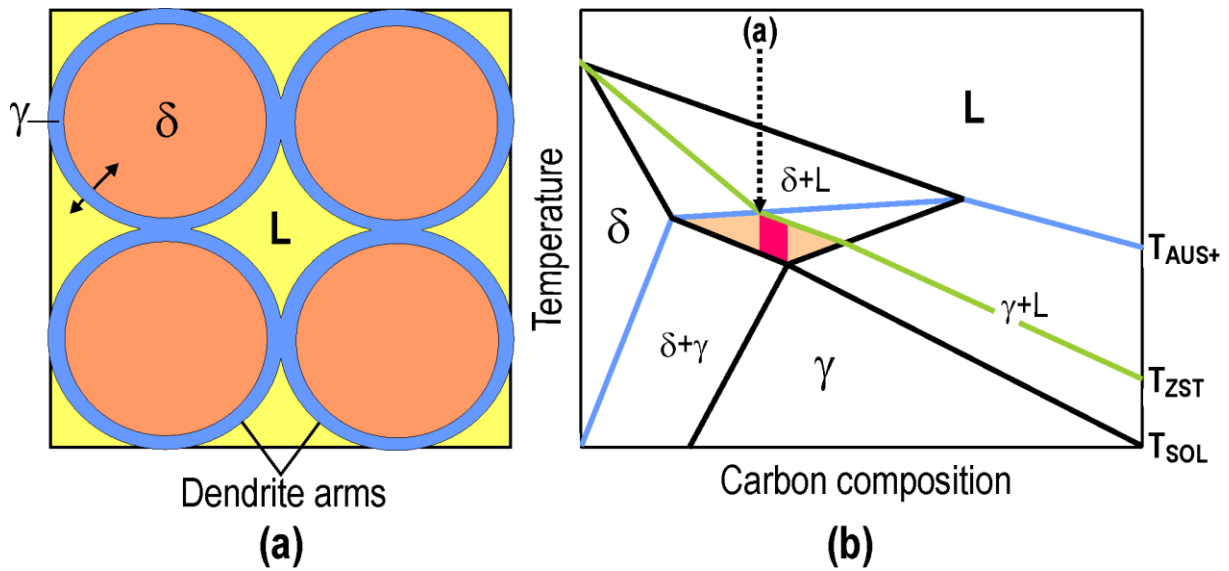


787

788 **Figure 12.** Detachment of the shell due to the delta ferrite/austenite transformation (a) and the
 789 red temperature zone, where shell growth is disturbed (b). **The worst cases are in the red zone.**

790 Temperature T_{s30} denotes $T_{SOL} - 30 \text{ }^\circ\text{C}$.

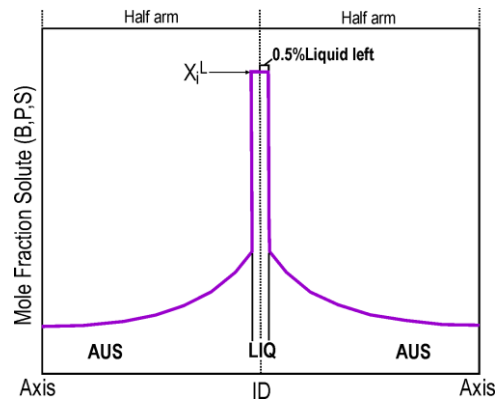
791



792

793 **Figure 13.** Background of quality index QI_{STR} . Formation of austenite layer between the liquid
 794 phase and ferrite just after strengthening (a) and the red temperature zone, where strengthening
 795 is disturbed (b). **The worst cases are in the red zone.**

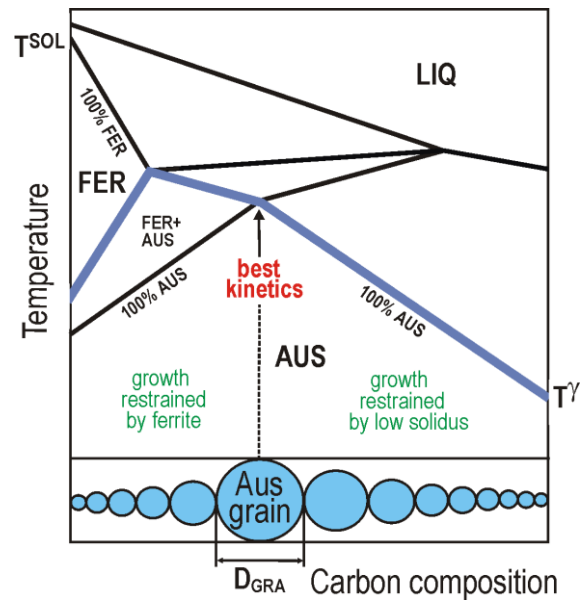
796



797

798 **Figure 3.** Background of quality index QI_{SOL} . Solute enrichments (e.g. S, P, B,) and the fraction
 799 of the liquid-state (Fe,Mn)S in the last liquid drop at the solidus (0.5% liquid left) for the
 800 derivation of QI_{SOL} index.

801

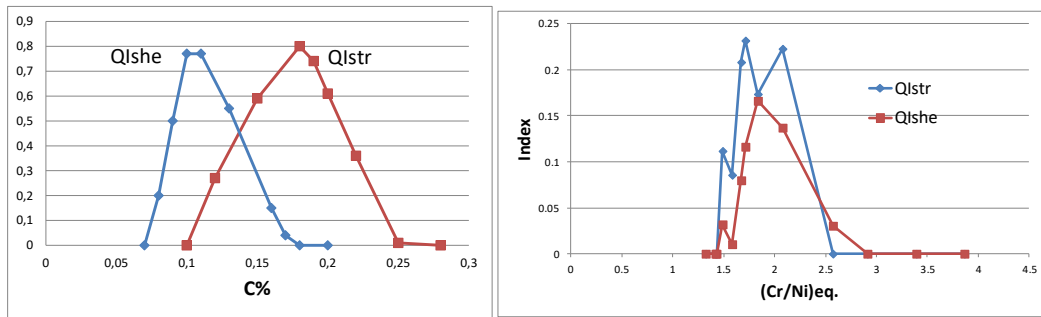


802

803 **Figure 4.** Background of quality index QI_{GRA} . Fastest austenite grain growth occurs in the
 804 composition region corresponding to 0.18 wt-% carbon with best possible kinetics (diffusion).

805

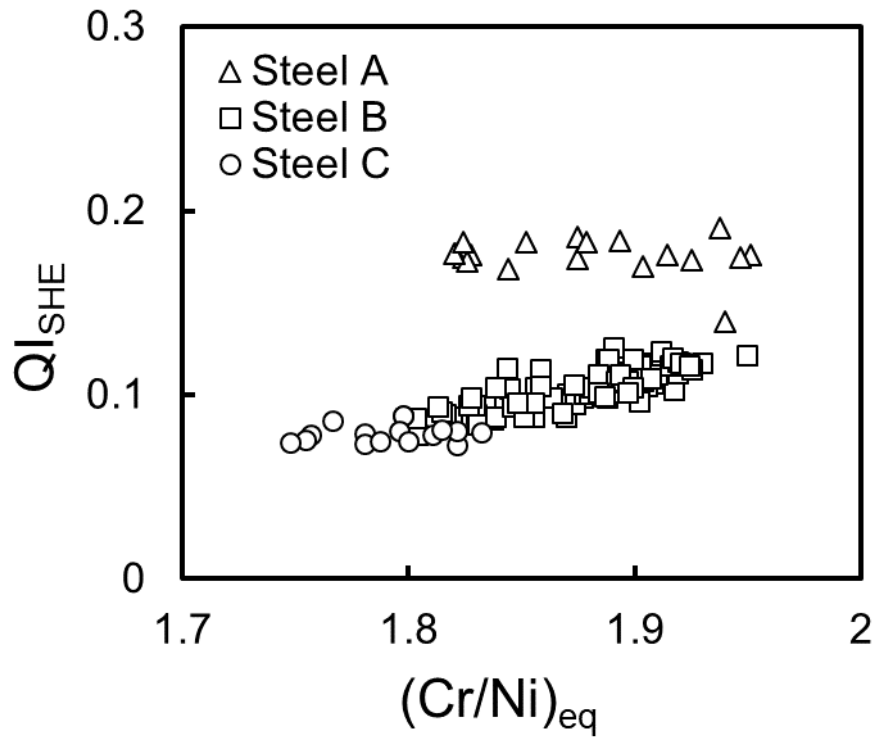
806



807

808 **Figure 5.** a) Indices QI_{STR} and QI_{SHE} for a fixed low alloyed steel composition with varying
 809 carbon content. The indices are partly overlapping, b) Corresponding QI_{STR} and QI_{SHE} indices
 810 for stainless steels showing nearly complete overlapping.

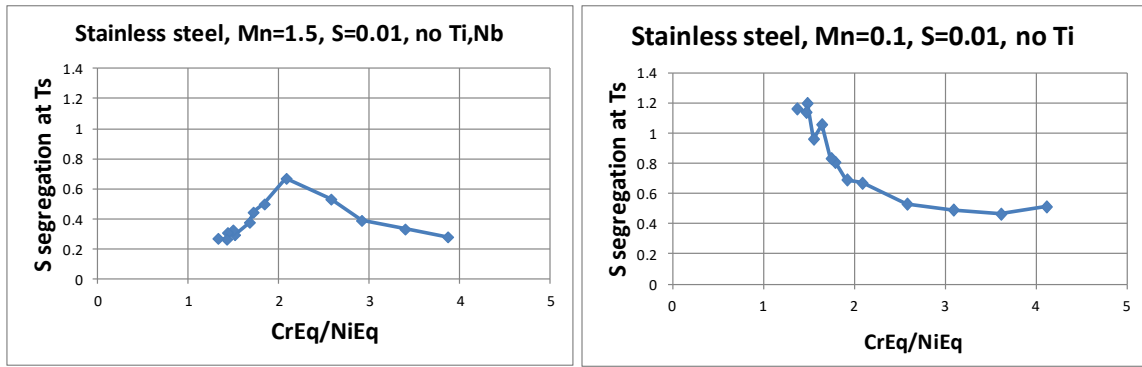
811



812

813 **Figure 14.** QI_{SHE} values for three stainless steel grades (A, B, C), which all are sensitive to
 814 bleeding, based on the statistical defect analysis made in the industry. Steel grade A is distinctly
 815 the most sensitive for bleeding and steel grade C is a bit less sensitive than grade B. QI_{STR} index
 816 gives very similar results.

817



818

819 **Figure 15.** Calculated segregation of sulfur in two different stainless steel grades. Left: not
 820 prone to hot cracking; right: very prone to hot cracking.

821

822 **LIST OF TABLES**

823

824 **Table 1.** Proposed main criterion indices for different types of **cracking** defects.

825 **Table 1.** Proposed main criterion indices for different types of **cracking** defects.

Defect	Criterion										
	Q _I SHE	Q _I STR	Q _I SOL	Q _I DUC	Q _I GRA	Q _I BUB	Q _I POR	Q _I COOL	Q _I COLD	Q _I HEAT	Tramp elements
Longitudinal surface cracking, facial and corner	X	X	X								
Transverse corner cracking	X	X		X	X						X
Bleeding	X	X									
Hot spots, depressions	X										
Near-surface pinholes						X					
Internal gas porosity, blowholes							X				
Star cracks	X			X							X
Cracking during cooling after continuous casting								X			
Cold cracking									X		
Cracking during reheating in the reheating furnace										X	

826